P type porous silicon resistivity and carrier transport

S. Ménard,[1,a] A. Fèvre,[1,2] J. Billoué,[2] and G. Gautier[2]
[1]*STMicroelectronics, 10, rue Thalès de Milet, 37071 Tours Cedex 2, France*
[2]*Université François Rabelais de Tours, CNRS, CEA, INSA CVL, GREMAN UMR 7347, Tours, France*

(Received 21 April 2015; accepted 25 August 2015; published online 14 September 2015)

The resistivity of p type porous silicon (PS) is reported on a wide range of PS physical properties. Al/PS/Si/Al structures were used and a rigorous experimental protocol was followed. The PS porosity ($P_{\%}$) was found to be the major contributor to the PS resistivity (ρ_{PS}). ρ_{PS} increases exponentially with $P_{\%}$. Values of ρ_{PS} as high as 1×10^9 Ω cm at room temperature were obtained once $P_{\%}$ exceeds 60%. ρ_{PS} was found to be thermally activated, in particular, when the temperature increases from 30 to 200 °C, a decrease of three decades is observed on ρ_{PS}. Based on these results, it was also possible to deduce the carrier transport mechanisms in PS. For $P_{\%}$ lower than 45%, the conduction occurs through band tails and deep levels in the tissue surrounding the crystallites. When $P_{\%}$ overpasses 45%, electrons at energy levels close to the Fermi level allow a hopping conduction from crystallite to crystallite to appear. This study confirms the potential of PS as an insulating material for applications such as power electronic devices. © *2015 AIP Publishing LLC*. [http://dx.doi.org/10.1063/1.4930222]

I. INTRODUCTION

Porous silicon (PS) is widely studied for many application domains such as optoelectronics,[1,2] photonics,[3,4] sensors,[5,6] microsystems,[7,8] and biomedical.[9,10] Indeed, PS shows electrical and thermal insulating properties and a huge chemical reactivity due to its high specific surface area. In particular, many studies dedicated to PS were published in the field of electronics, mainly for RF or DC insulation purposes.[11–15] Recently, it was proposed by our group to integrate PS in junction terminations of power semiconductor devices.[16] The PS electrical conductivity can actually be close to those of a good insulator, and existing doping profiles in AC switches are suitable for the PS formation. Despite the vast literature dealing with PS electrical properties, relations between different experiments are often difficult to establish. Indeed, the diversity of PS morphologies, the number of process parameters that have an influence on its features, and the wide variety of available characterization method tend to complicate the analysis of investigations. This observation is especially applicable to the PS conductivity as discussed by Ram[17] and further in this paper. On the contrary, PS dielectric permittivity is generally better described.[18] Therefore, the purpose of this paper is to provide an exhaustive study of the PS resistivity (ρ_{PS}). In particular, the evolution of ρ_{PS} with the porosity will be analyzed in details. We will focus on PS layers grown from p type substrate with thicknesses higher than 10 μm, as required by the targeted application. Moreover, the experimental protocol (fabrication and characterization) will be kept constant as much as possible. From these results, some models for conduction mechanisms will be proposed.

II. EXPERIMENTAL PROCEDURE

All the samples were prepared from 2 in. wafers with a thickness of 250 μm. Three (111) p type substrate resistivities (ρ_{Si}) were considered (p^- for a range of 6–12 Ω cm, p for 80–120 mΩ cm, and p^+ for 10–15 mΩ cm) in order to target different PS morphologies. The PS was formed by anodic etching carried out in a double-tank anodization cell filled with a 30% HF-H_2O-acetic acid electrolyte. The use of acetic acid was found to be an efficient additive (wetting agent) in previous works.[19,20] For resistivities higher than 20 mΩ cm, a boron doping (p^+) was previously implemented on the back side. Indeed, an ohmic contact is required on the cathodic face of the silicon substrate to ensure the formation of a homogeneous PS layer. This p^+ doping was achieved through Spin On Dopant (SOD) diffusion followed by a 1 h long diffusion annealing at 1000 °C in N_2. The anodization was then performed. Current densities (J_{ano}) and anodization durations (D_{ano}) were varied in the ranges of 10–150 mA/cm^2 and 5–105 min, respectively. Using these conditions, the PS layer thicknesses (t_{PS}) varied from 15 to 70 μm and porosities ($P_{\%}$) were between 25% and 75%. More details are given in Table I. $P_{\%}$ was assessed thanks to the gravimetric method, while a profilometer was used for t_{PS}. As these measurements are destructive, they were performed on witness wafers, processed in the same

TABLE I. Physical properties of the PS resulting from the anodization of the three p^-, p, and p^+ Si substrates.

Si	ρ_{Si} (Ω cm)	J_{ano} (mA/cm^2)	D_{ano} (min)	t_{PS} (μm)	$P_{\%}$ (%)	Morphology
p^+	0.05–0.015	10–100	6–25	15–30	25–50	Mesopores
p	0.08–0.12	10–150	5–36	15–45	40–65	Mesopores
p^-	6–12	15–150	5–105	20–70	60–75	Filled macropores

[a]Author to whom correspondence should be addressed. Electronic mail: samuel.menard@st.com. Tel.: +33(0) 47 42 40 00.

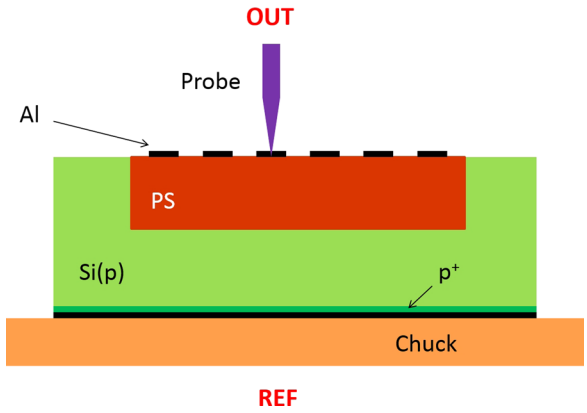

FIG. 1. Al/PS/Si/Al structure used to study the PS resistivity. The bias is applied on the PS side (OUT) and the chuck is used as the reference potential (REF).

way as the analyzed samples. After the anodization, wafers were rinsed with deionized water and dried in the ambient air on a hot plate at 150 °C. To stabilize the PS, all wafers were annealed during 1 h at 350 °C in a N_2 rich atmosphere (a slight oxidation can occur). Finally, a thick aluminum (Al) layer was deposited through Physical Vapor Deposition (PVD) on both faces of the wafer and a photolithographic process was used on the PS side to define circular patterns with a diameter of 0.5 mm. Al wet or dry etching was used without any impact on results. The former method used a solution that mixes acetic, nitric, and phosphoric acids with water. The latter one employed a Cl_2:C_2H_4 plasma. Note that dry etching involves an additional fusion of the masking resin (1 min at 180 °C). The resulting Al/PS/Si/Al structure is represented in Figure 1.

ρ_{PS} was extracted through I-V plots obtained with a Keithley 4200 semiconductor analyzer. As described in Figure 1, the bias (OUT) was applied on the PS side, while the back of the sample (i.e., the chuck) was used as a reference terminal (REF). Each sample was assessed with four characterization patterns. The test sequence was defined as follows: from 0 to $\mp$ 10 V (reproduced twice) and then from 0 to $\pm$10 V (reproduced twice), and no significant impact of the starting bias sign was observed. Five characterization temperatures were considered: 30, 50, 100, 150, and 200 °C. All measurements were done in the ambient air, meaning that there was no control of the humidity (RH). Depending on the analyzed samples, RH was between 10% and 80%. It has been shown that the PS electrical properties strongly depend on RH,[21,22] so all sample characterization campaigns were started at 200 °C and ended at 30 °C. With such a procedure, no water remained in the pores at the beginning of the test sequence. Therefore, the effect of RH on results is reduced.

III. PHYSICAL CHARACTERIZATION

t_{PS} and $P_{\%}$ ranges obtained for the three p^-, p, and p^+ substrates are summarized in Table I. A mesoporous texture is observed for p^+ type samples as described in Figure 2(a). The average pore diameter is approximately 10 nm. The same kind of mesoporous morphology is obtained with p type but the pore diameter seems to be smaller (Figure 2(b)). In the case of p^- substrates, the undulations visible at the PS/Si interface suggest the presence of neighboring macropores (Figure 2(c)). They are filled with mesoporous PS. All these results are consistent with previous studies reported in the literature.[23–25]

It can also be noticed that a thin surface layer (SL), due to pore nucleation, may be present on samples issued from the p^- and p substrates. Its thickness is in the order of several micrometers. A typical example, coming from a p^- substrate ($J_{ano} = 25$ mA/cm^2 and $D_{ano} = 35$ min), is given in Figure 3. Two zooms of TEM cross sections are added: the first focuses on the top of SL, while the second focuses at the interface between SL and the PS. The morphological differentiation between both layers is clearly distinguishable.

IV. I–V MEASUREMENTS AND RESISTIVITY EXTRACTION PROTOCOL

As explained in the experimental section, I–V plots were used to extract ρ_{PS}. Because of the presence of different interfaces in the Al/PS/Si/Al structure, and in particular, the ones with PS, the I–V interpretation is not immediate. In the case of p type PS, the Al/PS interface is generally considered

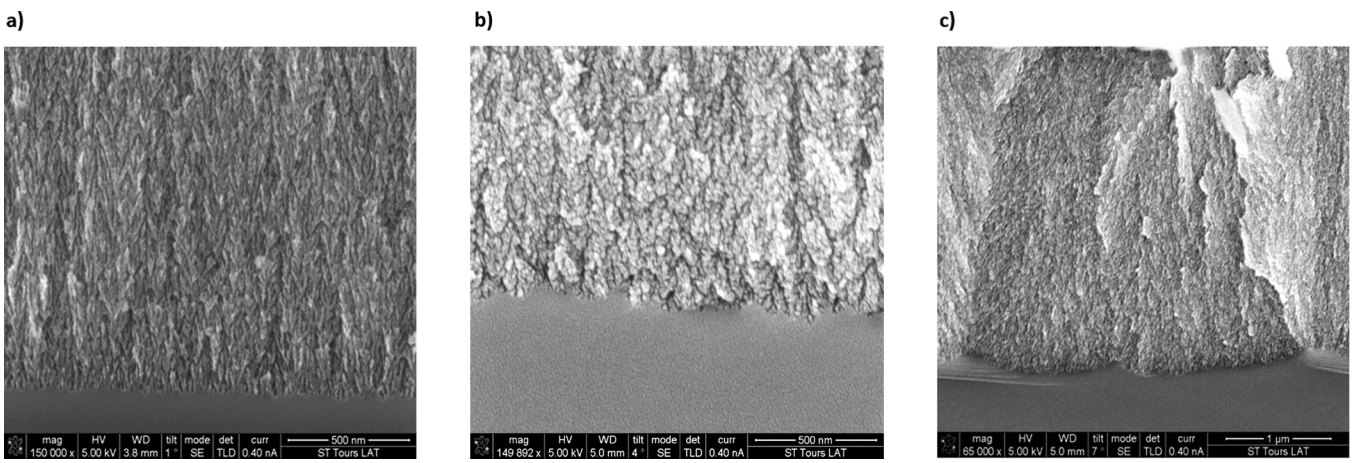

FIG. 2. MEB cross-section views of the PS morphologies stemming from the substrates with three different resistivities: (a) 10–15 mΩ cm, (b) 80–120 mΩ cm, (c) 6–12 Ω cm.

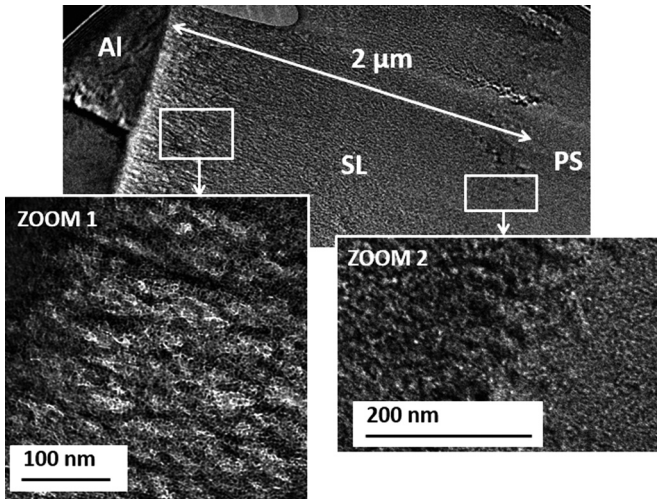

FIG. 3. TEM observations of SL present on the p^- sample processed with $J_{ano} = 25\,mA/cm^2$ and $D_{ano} = 35\,min$. The SL thickness is 2 μm. Zoom 1 is done on top of SL and zoom 2 focuses at its interface with the PS.

as ohmic because of the high surface state concentration on the pore walls, which screens the internal electric fields resulting from the barrier potential between Al and PS.[26] Nevertheless, the presence of an intermediate layer could induce a rectifying behavior.[21,27–29] Furthermore, when $P_{\%}$ is low, PS is partially depleted and the nature of the contact becomes dependent on the Si features.[30–33] Generally, the PS/Si interface (with p type PS) is assimilated to a Schottky diode, where the PS plays the role of the metal.[26] Thus, when a negative voltage is applied on the PS side, the diode is forward biased. However, if the PS resistance is high, the rectifying phenomenon is strongly attenuated. Moreover, for small crystallites (lower than 5 nm), there is an increase of the PS gap.[34–36] Therefore, the PS/Si interface could also be modeled as a heterojunction. In general, a p isotype configuration is proposed.[22,37]

Figures 4–6 show typical I–V results, respectively, from the p^-, p, and p^+ substrates. The direct bias (negative voltage applied on the PS side) is systematically represented with a full line, while a dotted one was chosen for the reverse

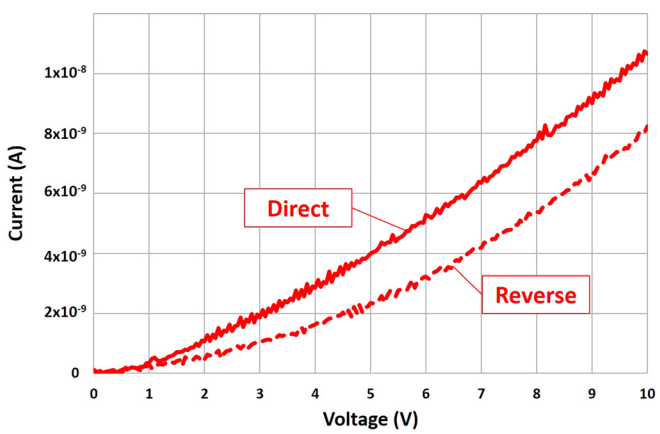

FIG. 4. Typical I–V plot obtained on the p^- substrate with $J_{ano} = 100\,mA/cm^2$ and $D_{ano} = 15\,min$. The temperature of measurement was 30 °C. The direct and reverse curves are represented in full and dotted lines, respectively.

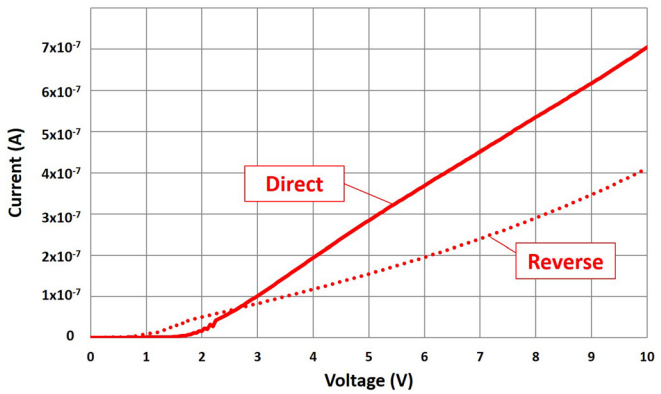

FIG. 5. Typical I–V plot obtained on the p substrate with $J_{ano} = 25\,mA/cm^2$ and $D_{ano} = 30\,min$. The temperature of measurement was 30 °C. The direct and reverse curves are represented in full and dotted lines, respectively.

configuration. For the p^- and p cases (Figures 4 and 5, respectively), two zones are visible: a current limiting region at low voltages followed by a more linear trend. The first part of the plot is likely to be the consequence of the SL existence, while the second one reflects the PS conductivity. Furthermore, it has to be noticed that direct and reverse regimes are asymmetrical. Depending on the physics at both PS interfaces, the direct bias may involve higher currents than the reverse one or not. For p^+ samples, a more classical ohmic law is visible (Figure 6). In addition, both direct and reverse plots are quasi symmetric. Finally, it can also be noticed that for higher voltages (>10 V), nonlinear effects may be observed. They could be attributed to Space Charge Limited Current (SCLC)[22,32,38–40] or Poole Frenkel conductions.[41]

To conclude this section, I–V curves are due to complex transport mechanisms. Thus, we chose to extract our ρ_{PS} data from the direct regime, overall more stable. We limited the analysis to the highest investigated biases, where linear behaviors are generally observed. Then, we fitted our experimental results with simple affine laws, knowing that some voltage dependencies can occasionally affect the accuracy of the results.

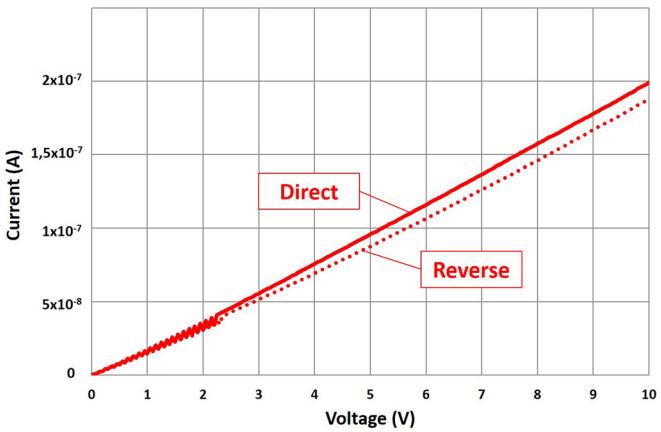

FIG. 6. Typical I–V plot obtained on the p^+ substrate with $J_{ano} = 50\,mA/cm^2$ and $D_{ano} = 15\,min$. The temperature of measurement was 30 °C. The direct and reverse curves are represented in full and dotted lines, respectively.

V. PS RESISTIVITY MEASUREMENTS AND DISCUSSION

All ρ_{PS} extracted at 30 °C are plotted in Figure 7 as a function of $P_{\%}$. The p^-, p, and p^+ substrates, respectively, with high, medium, and low porosities (see Table I for details) are represented with diamond, square, and triangle symbols. An increase of ρ_{PS} with $P_{\%}$ is observed. The global trend follows an exponential law as indicated by the full black line. The results of Bouaïcha *et al.*[42] (dotted line), Khardani *et al.*[43] (dotted and dashed line), and Lee *et al.*[44] (dashed line) are also included in the graph. Bouaïcha *et al.* worked on vertical Al/PS/Si/Al structures processed from a p-type substrate with $\rho_{Si} = 1\ \Omega$ cm. For high $P_{\%}$, there is a consistency with our results. However, by decreasing $P_{\%}$, a discrepancy appears between the two studies. Overall, the trend of resistivity reported in Ref. 42 remains exponential but with more gentle slopes. It is important to notice that no information is given about the procedure used to extract ρ_{PS}, and I–V curves are nonlinear. By analogy with the numerous publications related to this type of mesoporous morphology, the authors ascribe this behavior to the rectifying effect brought by the PS/Si interface. Furthermore, a post-metallization annealing was performed (at 500 °C for 1 min). This treatment may also affect the PS structure and its resistivity. Möller *et al.*[45] and Balagurov *et al.*,[38] for example, reported ρ_{PS} changes over several decades depending on the applied annealing temperature. This behavior is attributed to the removal of the hydrogen passivating the pore walls during the anodization and to oxidation.

Khardani *et al.* also carried out PS resistivity measurements but for vertical self-supported PS structures, that is to say, PS membranes removed from the initial substrate. The initial p type substrate had a resistivity of 20 mΩ cm, probably resulting in a mesoporous structure. In fact, one might expect similarities with the triangular points reported in Figure 7, which is not the case. The results obtained by Khardani *et al.* are found by far smaller and the variation with $P_{\%}$ is slight. The authors declared that they have obtained linear I–V. The ohmic character of the contact on PS was guaranteed by an Au deposit (0.2 μm) followed by a 2 min long annealing at 450 °C. It is possible that this treatment, and more broadly the entire manufacturing process knowing the sample specificity, has led to a structural modification of the PS. Note also that several studies on self-supported PS samples showed a strong impact of the external environment on the PS electrical properties during characterization.[27,32]

Lee *et al.*[44] also proposed a study of ρ_{PS} extracted from self-supported PS samples with various porosities from 30% to 75%. The initial p type substrate resistivity was in the range of 5–10 Ω cm. The authors do not disclose any information about the morphology of their PS, and it is quite possible that it is similar to that presented in Figure 2(c), namely, mesoporous silicon with typical pore sizes smaller than 10 nm. Whereas at low $P_{\%}$, the results of Lee *et al.* are consistent with our study, at higher $P_{\%}$ both trends start to deviate. The authors stated that ρ_{PS} comes from linear I–V measured in vacuum using coplanar top electrodes. The anisotropy of the structure and, as a consequence, of the electrical properties, could explain these differences.

Finally, many discrepancies are observed between the ρ_{PS} value of these four studies, thus demonstrating the importance of the sample fabrication process and characterization conditions. But, all of them converge on one point: ρ_{PS} is tunable through $P_{\%}$ and 5 to 10 orders of magnitude are gained on the resistivity compared to the initial substrate.

The exponential increase of ρ_{PS} with $P_{\%}$ was confirmed for temperatures from 30 to 200 °C. This trend is illustrated in Figure 8 representing ρ_{PS} as a function of $P_{\%}$ for different temperatures. In addition, a decrease of ρ_{PS} with temperature is also observed. Actually, ρ_{PS} is thermally activated as it will be discussed more deeply in Section VI. Three orders of magnitude stand between the results at 30 °C from 200 °C ones. In the scope of the targeted application, it is important to note that resistivities higher than 1×10^9 and $1 \times 10^6\ \Omega$ cm,

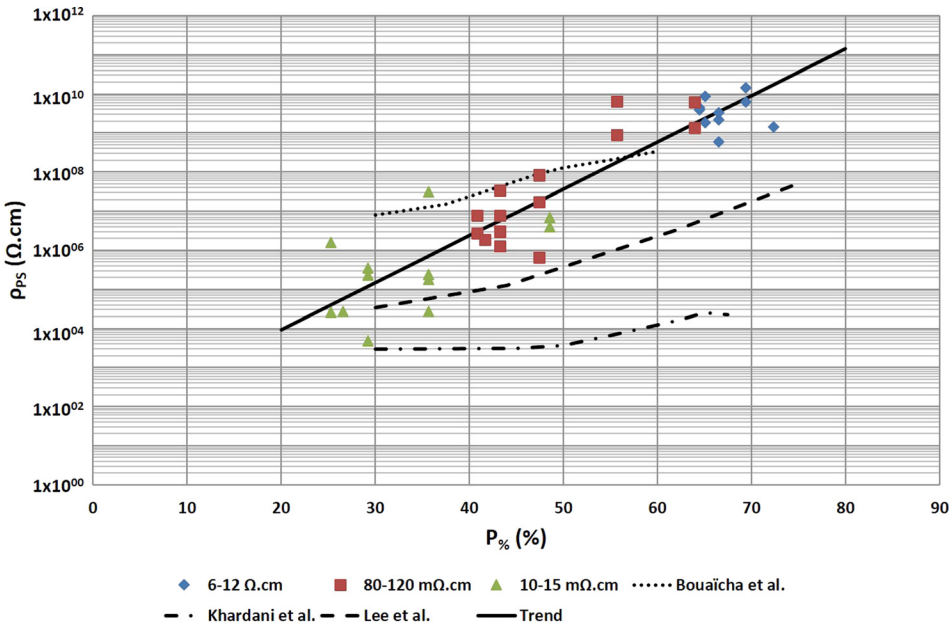

FIG. 7. ρ_{PS} versus $P_{\%}$ at 30 °C for the three considered substrates (diamond, square, and triangle symbols, respectively, for p^-, p, and p^+ samples). The full black line indicates the global exponential trend of the results. The data of Bouaïcha *et al.* (dotted line), Khardani *et al.* (dotted and dashed line), and Lee *et al.* (dashed line) are also represented.

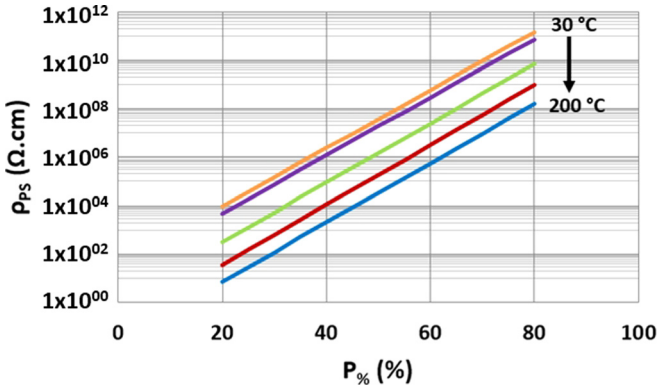

FIG. 8. ρ_{PS} versus $P_{\%}$ at 30, 50, 100, 150, and 200 °C. The global exponential trend is represented for each set of data.

respectively, at 30 and 200 °C, could be reached if $P_{\%}$ exceeds 60%, thus confirming the efficient insulator role the PS can play.

VI. TRANSPORT IN PS

As mentioned in Section V, ρ_{PS} was found to be thermally activated. The example of a p^- sample ($J_{ano} = 15$ mA/cm^2 and $D_{ano} = 105$ min), for which the Arrhenius law, characterized by the activation energy E_A and the pre-factor ρ_0, is given in Figure 9. It has also to be noticed that some double activation phenomena were observed (only for p^- and p substrates). Indeed, an increase of E_A can be observed from the lower temperatures to the higher ones in some marginal cases.

More data about transport in PS can be deduced from E_A and ρ_0 by using the Meyer Neldel formalism[46]

$$\ln\left(\frac{1}{\rho_0}\right) = B_{MNR} + \frac{E_A}{E_{MNR}}. \quad (1)$$

B_{MNR} and E_{MNR} are constant values representative of a given transport mechanism. By following this principle and by gathering several data coming from the literature, Lubianiker and Balberg[46] concluded in their work that two kinds of conductions can operate in PS.

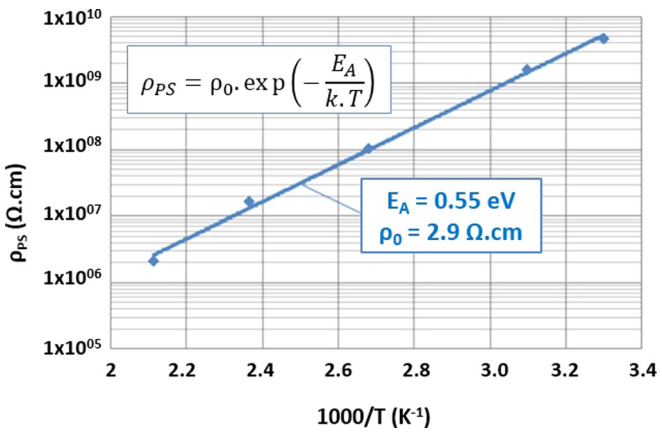

FIG. 9. Evidence of thermal activation of ρ_{PS} for a p^- sample processed with $J_{ano} = 15$ mA/cm^2 and $D_{ano} = 105$ min. The Arrhenius law is recalled in the inset.

The same kind of analysis was done on the basis of our E_A and ρ_0 data. The result is presented in Figure 10. As for Lubianiker and Balberg, two laws can be identified. The first one is indicated by the dashed line in Figure 10. It includes p samples with $P_{\%}$ lower than 45% and all the values obtained from p^+ substrates. It is similar to that obtained by Lubianiker and Balberg. E_{MNR}/B_{MNR} couples have indeed very close values: 41.1 meV/$2.6 \times 10^{-3}\,\Omega^{-1}\,cm^{-1}$ in our case compared to 50 meV/$7.2 \times 10^{-3}\,\Omega^{-1}\,cm^{-1}$ for Lubianiker and Balberg. This similarity indicates that the transport of carriers in the PS layer could happen in the tissue surrounding the crystallites, through band tails and deep centers, as observed for hydrogenated amorphous silicon. Such a conduction mechanism is the consequence of traps resulting from the presence of hydrogen and oxygen on the pore surfaces. Indeed, considering the low temperature sample preparation (lower than 350 °C), we may expect that both hydrogen and oxygen are present.[45] Hydrogen related traps may involve local electric fields, which lead to the formation of band tails.[47] Oxygen related traps may involve deep levels. Ben Chorin *et al.*[26] have reported a density of states of about $1 \times 10^{19}\,cm^{-3}\,eV^{-1}$ at the Fermi level. Once activated, carriers move from site to site in the band tails.

The second law obtained in the scope of this work is indicated by a dotted line in Figure 10. It includes p samples having $P_{\%}$ higher than 45% and the p^- wafers. It shows very different characteristics compared to that obtained by Lubianiker and Balberg. The E_{MNR}/B_{MNR} couple was estimated to be 33.4 meV/$6 \times 10^{-8}\,\Omega^{-1}\,cm^{-1}$, while Lubianiker and Balberg reported 166 meV/$2.2 \times 10^{-5}\,\Omega^{-1}\,cm^{-1}$. This discrepancy could be explained by the small amount of data constituting the second law derived by Lubianiker and Balberg. In particular, a reference is made to the work of Kocka *et al.*[48,49] This team has worked on three different p-type substrates (resistivity 15, 4, and 0.3 Ω cm). They characterized self-supported PS samples. Contact was made with a very special holder. The resulting I–V characteristics were not linear. So, the ρ_{PS} data disclosed by the authors are dependent on the bias voltage. Lubianiker and Balberg only considered in their analysis ρ_{PS} values extracted at 39 V. As a consequence, the sample preparation and the ρ_{PS} extraction methodology discussed by Kocka *et al.* stand out very clearly from our work. If we add three other sources cited by

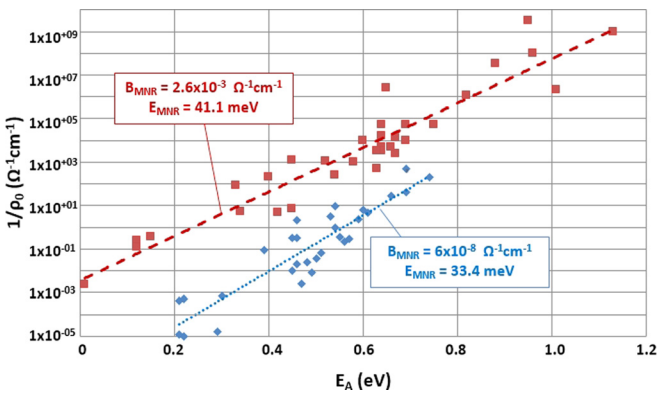

FIG. 10. Meyer Neldel formalism applied to E_A and ρ_0 data coming from the p^-, p, and p^+ substrates discussed in this paper.

Lubianiker and Balberg in the definition of the second law, we obtain consistent results with the dotted line of Figure 10. These three publications include that of Ben Chorin *et al.*,[50] who advocate a hopping conduction through energy states close to the Fermi level. Thus, this inter-crystallite carrier transport probably governs the conduction of the second half of our PS samples.

VII. CONCLUSIONS

The objectives of this paper were to analyze deeply the PS resistivity (ρ_{PS}). A focus was done on p-type mesoporous silicon. This choice was driven by the possibility to develop innovative junction terminations for power semiconductors devices. In this context, Al/PS/Si/Al structures were prepared on the basis of different substrate resistivities in order to cover a wide range of PS physical properties (porosity and morphology). A rigorous experimental procedure (sample processing and characterization) was followed. In many cases, this point limits the comparison between the studies on ρ_{PS} that have been published until now. In particular, we showed that ρ_{PS} tends to increase exponentially with the porosity ($P_{\%}$) without any impact of the morphology. At the ambient temperature, resistivities higher than 1×10^9 Ω cm for $P_{\%}$ exceeding 60% were measured from 30 to 200 °C, the same trend was observed; however, a decrease of three decades was observed. These results confirm the interest of PS as an insulator for electronic applications. Furthermore, ρ_{PS} was found to be thermally activated. By carefully analyzing this property, it was possible to collect data on the carrier transport mechanisms in PS. It was shown that for $P_{\%}$ lower than 45%, the conduction occurs through band tails and deep levels in the tissue surrounding the crystallites. When $P_{\%}$ exceeds 45%, electrons at energy levels close to the Fermi level allow a hopping conduction from crystallite to crystallite to appear.

ACKNOWLEDGMENTS

The authors would like to express their sincere gratitude to the staff of CERTeM technological platform and of the technology analysis laboratory at STMicroelectronics in Tours for their precious help with sample manufacturing and electrical characterization. The authors also acknowledge the financial support from BPI France through the "Projet Investissement d'Avenir (PIA) Tours 2015."

[1]A. Prasad, S. Balakrishnan, S. Jain, and G. Jain, J. Electrochem. Soc. **129**, 596 (1982).
[2]J. Anto Pradeep, P. Gogoi, and P. Agarwal, J. Non-Crystall. Solids **354**, 2544 (2008).
[3]U. Grüning, V. Lehmann, and C. Engelhardt, Appl. Phys. Lett. **66**, 3254 (1995).
[4]P. Ferrand, R. Romestain, and J. C. Vial, Phys. Rev. B **63**, 115106 (2001).
[5]S. Lewis, J. DeBoer, J. Gole, and P. Hesketh, Sens. Actuators, B **110**(1), 54 (2005).
[6]R. C. Erson, R. S. Muller, and C. W. Tobias, Sens. Actuators **23**, 835 (1990).
[7]P. Steiner and W. Lang, Thin Solid Films **255**, 52 (1995).
[8]F. Müller, A. Birner, J. Schilling, U. Gösele, C. Kettner, and P. Hänggi, Phys. Status Solidi A **182**, 585 (2000).
[9]A. Angelescu, I. Kleps, M. Mihaela, M. Simion, T. Neghina, S. Petrescu, N. Moldovan, C. Paduraru, and A. Raducanu, Rev. Adv. Mater. Sci. **5**, 440 (2003).
[10]A. Agrawal, B. Nehilla, K. Reisig, T. Gaborski, D. Fang, C. Striemer, P. Fauchet, and J. McGrath, Biomaterials **31**(20), 5408 (2010).
[11]R. Welty, S. Park, P. Asbeck, K. Dancil, and M. Sailor, in *Topical Meeting on Silicon Monolithic Integrated Circuits in RF Systems* (1998), p. 160.
[12]C. Nam and Y. Kwon, IEEE Microwave Guided Wave Lett. **7**, 236 (1997).
[13]Y. Watanabe, Y. Arita, T. Yokohama, and Y. Igarashi, J. Electrochem. Soc. **122**, 1351 (1975).
[14]S. Nakajima and K. Kato, Rev. Electr. Commun. Lab. **25**, 1039 (1977).
[15]K. Imai and H. Unno, IEEE Trans. Electron Devices **ED-31**(3), 297 (1984).
[16]S. Menard, A. Fèvre, D. Valente, J. Billoué, and G. Gautier, Nanoscale Res. Lett. **7**, 566 (2012).
[17]S. K. Ram, *Handbook of Porous Silicon*, edited by L. Canham (Springer, 2014), p. 144.
[18]T. I. Cox, in *Porous Silicon Data Review No. 18*, edited by L. Canham (INSPEC, London, 1997), p. 185.
[19]J. Semai, G. Gautier, and L. Ventura, J. Nanosci. Nanotechnol. **9**, 3652 (2009).
[20]G. Gautier, P. Leduc, J. Semai, and L. Ventura, Phys. Status Solidi C **5**(12), 3667 (2008).
[21]D. B. Dimitrov, Phys. Rev. B **51**(3), 1562 (1995).
[22]L. A. Balagurov, D. G. Yarkin, G. A. Petrovicheva, E. A. Petrova, A. F. Orlov, and S. Y. Andryushin, J. Appl. Phys. **82**(9), 4647 (1997).
[23]A. G. Cullis and L. T. Canham, "Visible light emission due to quantum size effects in highly porous crystalline silicon," Nature **353**, 335 (1991).
[24]V. Lehmann, R. Stengl, and A. Luigart, Mater. Sci. Eng., B **69–70**, 11 (2000).
[25]R. B. Wehrspohn, F. Ozanam, and J. N. Chazalviel, J. Electrochem. Soc. **146**(9), 3309 (1999).
[26]M. Ben Chorin, F. Möller, and F. Koch, J. Appl. Phys. **77**(9), 4482 (1995).
[27]D. Deresme, V. Marissael, D. Stievenard, and C. Ortega, Thin Solid Films **255**, 258 (1995).
[28]C. Cadet, D. Deresmes, D. Vuillaume, D. Stiévenard, A. Grosman, C. Ortega, J. Siejka, and H. Jürgen von Bardeleben, Mater. Sci. Forum **143–147**, 1475 (1994).
[29]S. P. Zimin, V. Kuznetsov, N. V. Perch, and A. V. Prokaznikov, Tech. Phys. Lett. **20**(11), 899 (1994).
[30]S. P. Zimin, Semiconductors **40**(11), 1350 (2006).
[31]R. C. Anderson, R. S. Muller, and C. W. Tobias, J. Electrochem. Soc. **138**(11), 3406 (1991).
[32]B. Remaki, C. Populaire, V. Lysenko, and D. Barbier, Mater. Sci. Eng., B **101**(1), 313 (2003).
[33]D. Stievenard and D. Deresmes, Appl. Phys. Lett. **67**(11), 1570 (1995).
[34]C. Delerue, M. Lannoo, G. Allan, and E. Martin, Thin Solid Films **255**, 27 (1995).
[35]J. Von Behren, T. Van Buuren, M. Zacharias, E. H. Chimowitz, and P. M. Fauchet, Solid State Commun. **105**(5), 317 (1998).
[36]S. Ogüt, J. R. Chelikowsky, and S. G. Louie, Phys. Rev. Lett. **79**(9), 1770 (1997).
[37]E. B. Kaganovich, E. G. Manolinov, and S. V. Svechnikov, Funct. Mater. **6**(3), 453 (1999); available at http://functmaterials.org.ua/contents/6-3/full/11full.pdf.
[38]L. A. Balagurov, D. G. Yarkin, and E. A. Petrova, Mater. Sci. Eng., B **69–70**, 127 (2000).
[39]N. Koshida, Y. Kiuchi, and S. Yoshimura, in *McGee Symposium of Photoelectric Image Devices* (1991), p. 377.
[40]L. A. Balagurov, S. C. Bayliss, A. F. Orlov, E. A. Petrova, B. Unal, and D. G. Yarkin, J. Appl. Phys. **90**(8), 4184 (2001).
[41]M. Ben-Chorin, F. Möller, and F. Koch, Phys. Rev. B **49**(4), 2981 (1994).
[42]M. Bouaïcha, M. Khardani, and B. Bessaïs, Mater. Sci. Eng., C **26**(2), 486 (2006).
[43]M. Khardani, M. Bouaïcha, W. Dimassi, M. Zribi, S. Aouida, and B. Bessaïs, Thin Solid Films **495**, 243 (2006).
[44]W. H. Lee, C. Lee, Y. H. Kwon, C. Y. Hong, and H. Y. Cho, Solid State Commun. **113**, 519 (2000).
[45]F. Möller, M. Ben Chorin, and F. Koch, Thin Solid Films **255**, 16 (1995).
[46]Y. Lubianiker and I. Balberg, Phys. Rev. Lett. **78**(12), 2433 (1997).
[47]L. K. Pan, H. T. Huang, and C. Q. Sun, J. Appl. Phys. **94**(4), 2695 (2003).
[48]A. Fejfar, I. Pelant, E. Sipek, J. Kocka, G. Juska, T. Matsumoto, and Y. Kanemitsu, Appl. Phys. Lett. **66**(9), 1098 (1995).
[49]J. Kocka, I. Pelant, and A. Fejfar, J. Non–crystall. Solids **198–200**, 857 (1996).
[50]M. Ben-Chorin, F. Möller, F. Koch, W. Schirmacher, and M. Eberhard, Phys. Rev. B **51**(4), 2199 (1995).